Article

Kinetics of Dimethoate, Malathion, and Chlorpyrifos Adsorption on Cellulose-derived Activated Carbons – Linking Performance to the Physicochemical Properties

Tamara Lazarević-Pašti [1,*], Ana Jocić [1], Vedran Milanković [1], Tamara Tasić [1], Nebojša Potkonjak [1], Stefan Breitenbach [2,3], Christoph Unterweger [2], Christian Fürst [2] and Igor A. Pašti [4]

[1] University of Belgrade, VINČA Institute of Nuclear Sciences - National Institute of the Republic of Serbia, Mike Petrovica Alasa 12-14, 11000 Belgrade, Serbia; lazarevictlj@yahoo.com; ana.jocic@vin.bg.ac.rs; vedran.milankovic@vin.bg.ac.rs; tamara.tasic@vin.bg.ac.rs; npotkonjak@vin.bg.ac.rs

[2] Wood K plus –Kompetenzzentrum Holz GmbH, Altenberger Strasse 69, 4040 Linz, Austria; s.breitenbach@wood-kplus.at; c.unterweger@wood-kplus.at; c.fuerst@wood-kplus.at

[3] Institute of Chemical Technology of Inorganic Materials (TIM), Johannes Kepler University Linz, Altenberger Strasse 69, 4040 Linz;

[4] University of Belgrade – Faculty of Physical Chemistry, Studentski trg 12-16, 11158 Belgrade, Serbia; igor@ffh.bg.ac.rs

* Correspondence: lazarevictlj@yahoo.com; tamara@vin.bg.ac.rs

Abstract: Due to the accumulation of pesticides in the environment, the development of efficient strategies for their removal is of utmost importance. Activated carbons are currently seen as excellent candidates for adsorptive pesticide removal based on several beneficial properties, like a large surface area, developed porosity, and low price. However, a deep link between materials' properties and performance is still elusive. Here we focus on the kinetics of three organophosphate pesticides removal, aliphatic dimethoate and malathion and aromatic chlorpyrifos, using a series of carefully prepared activated carbon fibers. Used adsorbents have a wide range of specific surface areas, pore size distributions, and elemental content, allowing the establishment of the link between physicochemical properties and their performance as adsorbents. We use data analysis tools to link these properties and discuss their different roles in the removal of three structurally different yet extremely dangerous pesticides. The obtained results can guide the synthesis of novel adsorbents or rationally select adsorbents for specific target pollutants based on the physicochemical properties of adsorbents and the chemical structure of pollutants.

Keywords: organophosphate pesticide; removal; adsorption; kinetics; textural properties

1. Introduction

Organophosphates (OPs) are the most commonly used group of pesticides and represent a global threat to the environment and humans [1-3]. They exert their toxicity towards animals due to the inhibition of acetylcholinesterase (AChE), one of the most important enzymes in the nervous system [4, 5]. Many methods for removing pesticides from the environment include adsorption, degradation, and microbiological treatment [6]. Among the mentioned processes, adsorption is most frequently used because it is effective, affordable, environmentally friendly and robust.

Carbon materials form a large group of materials with various textures, structures and properties. Due to their specific combination of physical and chemical properties, biocompatibility and diversity, their applications are numerous in all branches of science and engineering. The popularity of carbon materials increased enormously with the development of biomass-based carbon materials because of their versatile and highly porous structure availability and low cost [7]. In addition, by using waste biomass in carbon materials production, increasingly important sustainability/circularity aspects can be addressed.

 doi:10.20944/preprints202211.0449.v1

Several factors can influence the organic compounds' adsorption onto carbon materials, such as the nature of the adsorbent [8-10], the nature of the adsorbate [8, 9], and the solution conditions [8-10].

When it comes to the characteristics of the adsorbent, the main factors are the structure and size of pores, chemical surface area, specific surface area, pore volume, mesopore, micropore, and nanopore volume, presence of surface functional groups, and zero charge point (pH_{pzc}) [8, 9, 11]. As the pore size decreases, the adsorption strength increases as (1) the contact points between the adsorbate and the adsorbent surface increase [12] and (2) the adsorption potentials between opposite pore walls begin to overlap when the micropore width is less than approximately twice the adsorbate diameter, as suggested for gas (N_2) adsorption [13-14] and methyl tertiary-butyl ether and trichloroethene [15]. In addition, the adsorption capacity generally increases with a specific surface area due to the availability of adsorption sites [9], but this is certainly not a general case. The surface chemistry of activated carbon essentially depends on the content of heteroatoms, mainly on the range of oxygen complexes on the surface. It is considered that the surface oxygen complexes determine the surface charge, hydrophobicity, and electron density [10].

Characteristics of the adsorbate important for the adsorption process include pKa, functional groups present, polarity, molecular weight and size [8], solubility, and nature of the substituent if they are aromatic [10]. The size of the molecules controls the access of carbon pores, and solubility determines hydrophobic interactions. The pKa controls the dissociation of adsorption if it is an electrolyte. The aromatic ring substituent of adsorption molecules, as in the case of the graphene layer substituent, can pull or release electrons from it, which would affect the dispersion interactions between the adsorbate aromatic ring and the graphene layers in the adsorbent [10]. For example, Haghseresht et al.[8] showed that the dominant adsorption forces for the hydrophilic activated carbons were dipolar interactions for solutes in their molecular form. Dispersive forces were found to be dominant for basic hydrophobic carbons and the same type of adsorbates. However, dispersive forces were suggested as operative when the adsorbates are in their ionic forms, irrespective of the carbon surface type. For this study, p-cresol, p-nitrophenol, benzoic acid, nitrobenzene, and salicylic acid were used to probe the adsorption properties of carbons.

Solution conditions such as pH, ionic strength, and temperature also can affect the adsorption process [8-10]. Namely, the pH of a solution determines the carbon material surface charge and the electrolytes' dissociation or protonation [10]. When the pH of the solution is above the pH of zero charge of the carbon material, then the surface is negatively charged and can attract cations from the solution; otherwise, the carbon material surface is positive and attractive to anions [10, 11, 16, 17]. A higher pH_{pzc} value results in a higher adsorption rate in basic solutions. Similarly, in acidic solutions, a lower pH_{pzc} results in a higher adsorption rate [11, 16]. These conclusions have been derived for the case of reactive dyes, including methylene blue [16]. In addition, the pH of the solution also controls the dissociation or ionization of the electrolyte via its pK_a, where acidic electrolytes will be dissociated at $pH > pK_a$[10].

In the aqueous phase, van der Waals, induced-dipole, dipole-dipole, and donor-acceptor hydrogen binding forces are responsible for the binding and accumulation of chemical compounds on carbonaceous adsorbents [9]. Among different interactions, hydrogen and $\pi - \pi$ bonds, covalent and electrostatic interactions and the hydrophobic effect play an important role in adsorption [9, 18, 19].

Ionic strength is another key factor that controls electrostatic interactions. Whether attractive or repulsive, these interactions can be reduced by increasing the ionic strength of the solution. It is due to the screening effect of the surface charge produced by the added salt. Therefore, when the electrostatic interaction between the surface and adsorbate is repulsive or the surface concentration is high enough, increasing ionic strength will increase adsorption. In contrast, increasing the ionic strength will reduce adsorption when electrostatic interactions are attractive, or the surface concentration is low enough.

 doi:10.20944/preprints202211.0449.v1

Regarding the influence of temperature on the adsorption process, an increase in the intake of organic molecules is expected when the adsorption temperature decreases because adsorption is a spontaneous process. However, some examples show that the adsorbed amount increases with temperature [10].

While many different materials have been investigated as adsorbents, our understanding of the key materials' properties defining adsorption performance is still missing. This is likely due to the complexity of the process and the number of parameters influencing the adsorption process in a mutual interplay. Here we use a well-characterized series of activated carbon fibers to analyze the impact of their properties on the kinetics of chlorpyrifos, dimethoate, and malathion adsorption from aqueous solutions.

2. Results

2.1. Materials properties

This contribution aims to correlate the kinetics of pesticide adsorption to the adsorbents' physicochemical properties. Thus, the primary data we use here are given in **Table 1**. The materials studied in this work have already been investigated in terms of adsorption performance [20, 21]. Still, the focus was on the thermodynamic properties and the analysis of the impact of materials' properties on the adsorption capacities. One of the main conclusions was that specific surface area does not play a dominant role in determining adsorption capacity but rather pore volume and carbon and oxygen content. However, studied materials are micro- and mesoporous with different pore size distributions (**Table 1**, **Figure 1**). Thus, it is still unclear which portion of the total pore volume is responsible for the overall uptake of pollutants, particularly the kinetics of this process.

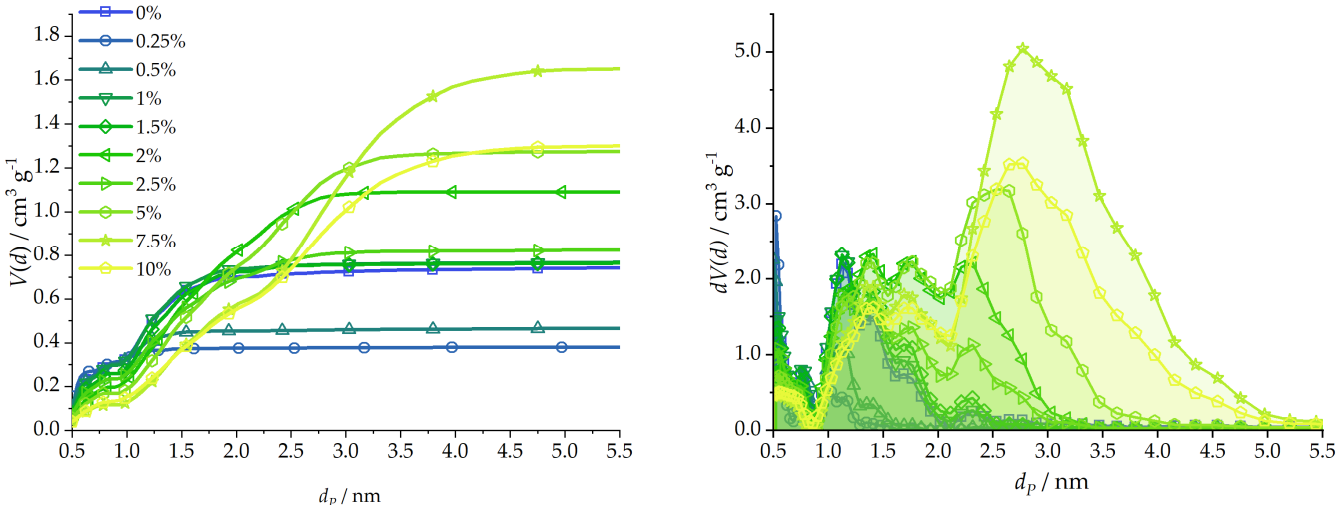

(**a**) (**b**)

Figure 1. (**a**) Integral pore volumes up to a given pore diameter function; (**b**) Common pore size distribution curves for studied adsorbents. Reproduced from [20] under Creative Commons License. The notation of samples is DAHP-X, where X is given in the figure legend.

Preprints (www.preprints.org) | NOT PEER-REVIEWED | Posted: 24 November 2022 doi:10.20944/preprints202211.0449.v1

Table 1. Adsorbents properties – pore volume integrated up to a given pore diameter, total pore volume (integrated up to d_P = 35 nm), surface area and elemental content determined using energy dispersive X-ray spectroscopy. The notation of samples is DAHP-X, where X stands for the amount of DAHP used for the impregnation step.

X =		**0.00%**	**0.25%**	**0.50%**	**1.00%**	**1.50%**	**2.00%**	**2.50%**	**5.00%**	**7.50%**	**10%**
Pores up	1 nm	0.348	0.335	0.339	0.343	0.297	0.271	0.274	0.198	0.137	0.160
to:	2 nm	0.702	0.375	0.454	0.738	0.723	0.857	0.696	0.754	0.580	0.559
(volume /	3 nm	0.725	0.377	0.459	0.759	0.756	1.086	0.813	1.200	1.180	1.021
$cm^3\ g^{-1}$)	4 nm	0.734	0.378	0.462	0.763	0.760	1.091	0.819	1.267	1.568	1.254
V_{tot}* / $cm^3\ g^{-1}$		0.757	0.383	0.472	0.774	0.770	1.094	0.833	1.291	1.681	1.322
S_{tot}** / $m^2\ g^{-1}$		1932	1016	1250	2037	2002	2556	2018	2718	2763	2718
Elementa	C / at.%	92.4±2.1	91.6±3.5	93.6±2.3	87.9±1.3	93.9±1.9	91.3±2.0	87.9±2.0	85.6±2.5	82.2±2.2	77.8±5.0
l	O / at.%	7.6±2.0	8.4±3.5	6.2±2.2	12±1.3	5.9±1.9	7.7±2.3	11.4±2.2	13.1±2.7	16.1±2.3	19.7±5.3
Content**	P / at.%	0	0.02±0.02	0.18±0.10	0.11±0.04	0.28±0.07	0.91±0.29	0.65±0.30	1.32±0.34	1.78±0.13	1.9±0.64

* Integrated up to 35 nm; ** Reference [20], reproduced under Creative Commons License.

As explained in previous publications addressing the adsorption capacities of the same series of ACFs [20, 21], these materials are particularly suitable for testing different hypotheses about the adsorption process. All these materials have been derived from the same precursor and have identical morphology (**Fig. 2**).

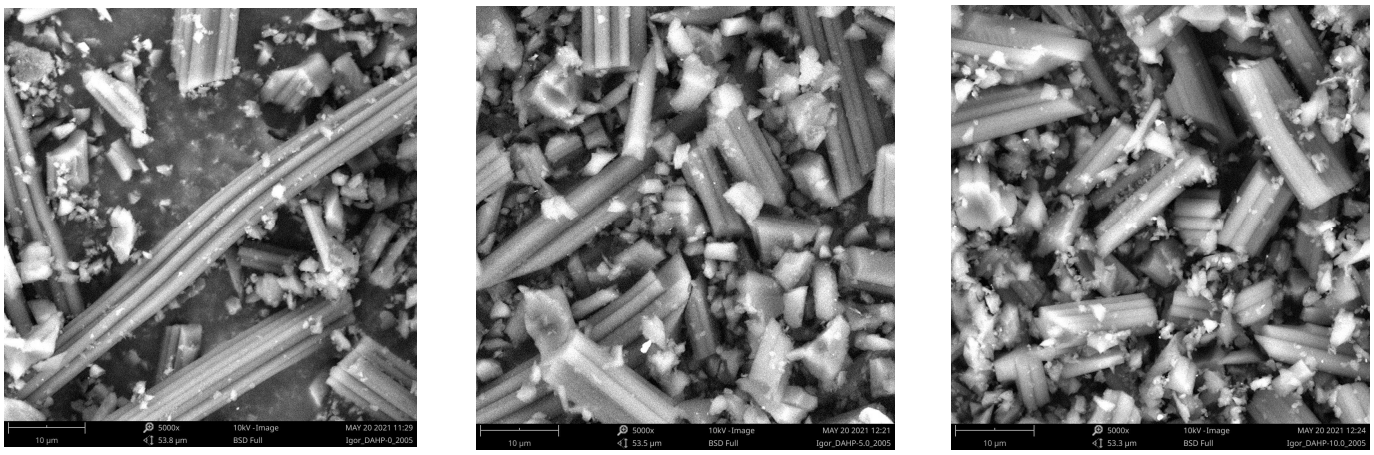

(**a**) (**b**) (**c**)

Figure 2. SEM images of(**a**) DAHP-0.00% sample; (**b**) DAHP-5.00% sample; (c) DAHP-10.00% sample. Magnification ×5,000, scale bar 10 μm, field of view 53.3 μm.

All the samples have undergone the same milling procedure, so the effects of morphology and size of particles on the adsorption performance can be excluded. Additionally, due to the same carbonization and activation temperatures, the Raman spectra of all the samples turned out to be identical [20]. Thus, the effects of the disorder degree can also be excluded. This leaves pore size distribution and elemental content (**Table 1**), effectively tuned by the amount of impregnating agent, DAHP, as the decisive properties which affect the adsorption kinetics.

2.2. Materials performance

In the forthcoming sections, we have processed adsorption data for chlorpyrifos, dimethoate, and malathion. First, adsorption was analyzed for up to 60 minutes, and the concentration of the pesticide remaining in the solution at a given moment of time was evaluated using UPLC analysis (Section 4). Then, the amount of adsorbed pesticide in a given moment of time (q_t) was fitted into the kinetic equations assuming kinetics obeying pseudo-first (Eq. 1) and pseudo-second-order (Eq. 2):

 doi:10.20944/preprints202211.0449.v1

$$\ln(q_e - q_t) = \ln(q_e) - k_1 t, \quad (1)$$

and

$$\frac{t}{q_t} = \frac{1}{k_2 q_e^2} + \frac{1}{q_e} t \quad (2)$$

where q_e is the equilibrium adsorption capacity, while k_1 and k_2 stand for the pseudo-first and pseudo-second rate order constants. The obtained rate order constants are presented in **Tables 2-4** for chlorpyrifos, dimethoate, and malathion.

From the value of k_1, the adsorption half-time ($t_{1/2}$) can be calculated as:

$$t_{1/2} = \frac{ln2}{k_1} \quad (3)$$

which gives the time upon which one half of the pesticide adsorption capacity is taken up by adsorbent.

2.2.1. Chlorpyrifos removal

The rate constants for chlorpyrifos removal are given in **Table 2**. It can be seen that the rate constants for pseudo-first-order reaction kinetics are determined with large uncertainties. In contrast, rate constants are determined more reliably for the pseudo-second-order kinetics. This is partially contributed by the fact that we have used a linearized form of the equation for the second-order kinetics. While linearized forms are easier to handle, they artificially increase the correlation coefficient [22]. However, here we are interested in the overall trends and connecting these trends to the materials' properties rather than determining highly accurate adsorption rate constants. In this sense, at first glance, there is no apparent trend in chlorpyrifos removal constants considering the overall trends in materials properties (**Table 1**) – an overall increase in total pore volume and an increase in O and P atomic content. Although the reliability of the pseudo-first-order constants is not high, it is possible to conclude that the half-times for chlorpyrifos adsorption are of the order of 10 min. This result is well in line with previous adsorption kinetics studies of different pesticides on carbon materials [23-25]. Minute ranges of chlorpyrifos adsorption half-times were reported for gamma radiation-modified activated carbon [26], while graphitic carbon nitride (g-C_3N_4) incorporated chitosan showed chlorpyrifos adsorption kinetics very similar to presented ACFs [27]. Nevertheless, half-times obtained here were much higher compared to, for example, the one found for chlorpyrifos removal by NU-1000 metal-organic framework, which was only 0.43 min [28].

Preprints (www.preprints.org) | NOT PEER-REVIEWED | Posted: 24 November 2022 doi:10.20944/preprints202211.0449.v1

Table 2. Rate constants for chlorpyrifos removal. The notation of samples is DAHP-X, where X represents the amount of DAHP used for the impregnation step. For the adsorption measurements, the chlorpyrifos concentration was 1×10^{-4} mol $dm^{-3,}$ while the adsorbents concentration was 0.1 mg ml^{-1} in each case.

X =	0.00%	0.25%	0.50%	1.00%	1.50%	2.00%	2.50%	5.00%	7.50%	10%
					Pseudo-1st order					
k_1/min^{-1}	0.054	0.034	0.0596	0.049	0.048	0.048	0.053	0.047	0.055	0.045
Δk_1/min^{-1}	0.022	0.012	0.0048	0.015	0.014	0.018	0.019	0.015	0.025	0.023
R^2	0.7206	0.75	0.98728	0.81	0.84	0.75	0.78	0.82	0.66	0.58
					Pseudo-2nd order					
k_2 / g mg^{-1} min^{-1}	0.0053	0.0086	0.0032	0.0028	0.0030	0.0052	0.0067	0.0045	0.0134	0.0085
Δk_2 / g mg^{-1} min^{-1}	7×10^{-4}	8×10^{-4}	2×10^{-4}	8×10^{-4}	7×10^{-4}	1×10^{-4}	1×10^{-4}	1×10^{-4}	2×10^{-4}	3×10^{-4}
R^2	0.9995	0.98	0.99996	0.998	0.998	0.9991	0.9995	0.998	0.9996	0.998

2.2.1. Dimethoate and malathion removal

In contrast to chlorpyrifos, which possesses an aromatic ring in its structure, dimethoate and malathion are aliphatic molecules. Nevertheless, the same general observations given for chlorpyrifos hold for dimethoate and malathion adsorption kinetics, as well. There are no apparent trends, and k_2 is determined with higher reliability compared to k_1. The half-times for dimethoate adsorption are in the range of 3.4-17.8 min. For malathion, the range is 1 min to 12.6 min. Similarly to chlorpyrifos, the estimated half-times for dimethoate adsorption on studied ACFs are in the range or lower compared to those which can be found in the literature or calculated on the basis of reported k_1, like for the case of KOH-modified *Thevetia peruviana* shell activated carbon [29]. The studied ACF are very efficient adsorbents for malathion removal and also possess better adsorption kinetics than some other carbons, like waste-derived activated carbons [30].

Table 3. Rate constants for dimethoate removal. The notation of samples is DAHP-X, where X stands for the amount of DAHP used for the impregnation step. For the adsorption measurements, dimethoate concentration was 1×10^{-4} mol $dm^{-3,}$ while the adsorbents concentration was 0.1 mg ml^{-1} in each case.

X =	0.00%	0.25%	0.50%	1.00%	1.50%	2.00%	2.50%	5.00%	7.50%	10%
					Pseudo-1st order					
k_1/min^{-1}	0.204	0.044	0.074	0.039	0.070	0.088	0.053	0.0368	0.055	0.142
Δk_1/min^{-1}	0.072	0.021	0.025	0.016	0.018	0.012	0.013	0.0026	0.011	0.020
R^2	0.64	0.53	0.65	0.72	0.78	0.95	0.85	0.98	0.88	0.94
					Pseudo-2nd order					
k_2 / g mg^{-1} min^{-1}	0.281	0.048	0.016	0.017	0.0343	0.0064	0.040	0.0069	0.030	0.092
Δk_2 / g mg^{-1} min^{-1}	6×10^{-3}	2×10^{-3}	1×10^{-3}	2×10^{-3}	6×10^{-4}	5×10^{-4}	3×10^{-3}	6×10^{-4}	3×10^{-3}	2×10^{-3}
R^2	0.99997	0.98	0.998	0.98	0.998	0.992	0.997	0.94	0.998	0.9998

Preprints (www.preprints.org) | NOT PEER-REVIEWED | Posted: 24 November 2022 doi:10.20944/preprints202211.0449.v1

Table 4. Rate constants for malathion removal. The notation of samples is DAHP-X, where X stands for the amount of DAHP used for the impregnation step. For the adsorption measurements, the concentration of malathion was 1×10^{-4} mol $dm^{-3,}$ while the adsorbents concentration was 0.1 mg ml^{-1} in each case.

X =	0.00%	0.25%	0.50%	1.00%	1.50%	2.00%	2.50%	5.00%	7.50%	10%
					Pseudo-1st order					
k_1/min^{-1}	0.055	0.49	0.70	0.402	0.234	0.214	0.149	0.143	0.064	0.223
Δk_1/min^{-1}	0.012	0.20	0.27	0.087	0.025	0.073	0.016	0.033	0.026	0.013
R^2	0.86	0.61	0.66	0.87	0.97	0.72	0.98	0.85	0.64	0.99
					Pseudo-2nd order					
k_2 / g mg^{-1} min^{-1}	0.0075	0.0214	0.0085	0.0608	0.1002	0.0754	0.0166	0.0070	0.0634	0.0097
Δk_2 / g mg^{-1} min^{-1}	2×10^{-4}	6×10^{-4}	5×10^{-4}	3×10^{-4}	7×10^{-4}	7×10^{-4}	3×10^{-4}	7×10^{-4}	4×10^{-4}	2×10^{-4}
R^2	0.998	0.996	0.98	0.9998	0.99999	0.99998	0.9997	0.9996	0.9998	0.998

3. Discussion

We turned to multiple linear regression analysis to investigate the impact of materials properties on the adsorbents' performances. It is a rather simple tool but can reveal some hidden links between dependent and independent variables, which can only be easily comprehended with the help of statistical tools. In short, it is assumed that the rate constants k_1 or k_2 can be presented as a linear combination of properties (x_i) given in **Table 1** with corresponding coefficients (A_i) as:

$$k = \sum_i A_i x_i. \quad (4)$$

Counter i is 1-4 to pore volumes up to 1, 2, 3, and 4 nm, respectively, 5 for total pore volume, and 6-8 for C, O, and P atomic content, respectively. The results of the linear regression analysis are given in **Figure 3**. Before the analysis, both k_1 and k_2 were multiplied by 100, while C and O contents were divided by 100 and 10, respectively, to scale all the quantities used in the analysis to similar orders of magnitude.

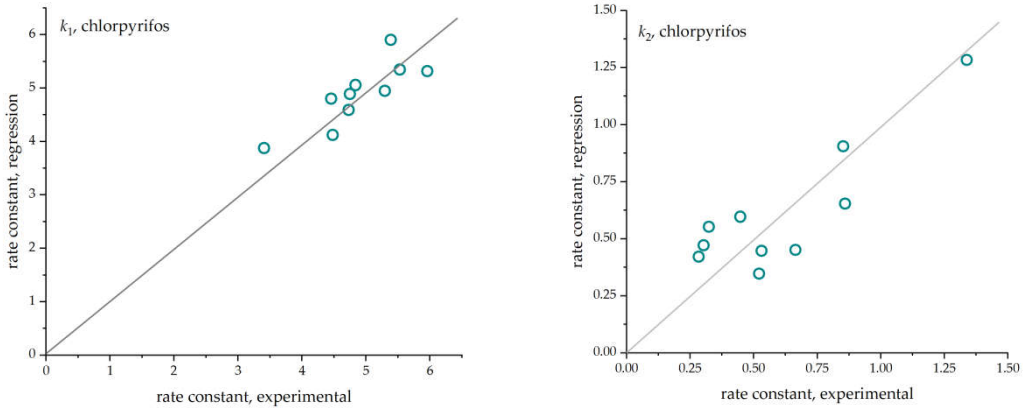

(**a**) (**b**)

Preprints (www.preprints.org) | NOT PEER-REVIEWED | Posted: 24 November 2022 doi:10.20944/preprints202211.0449.v1

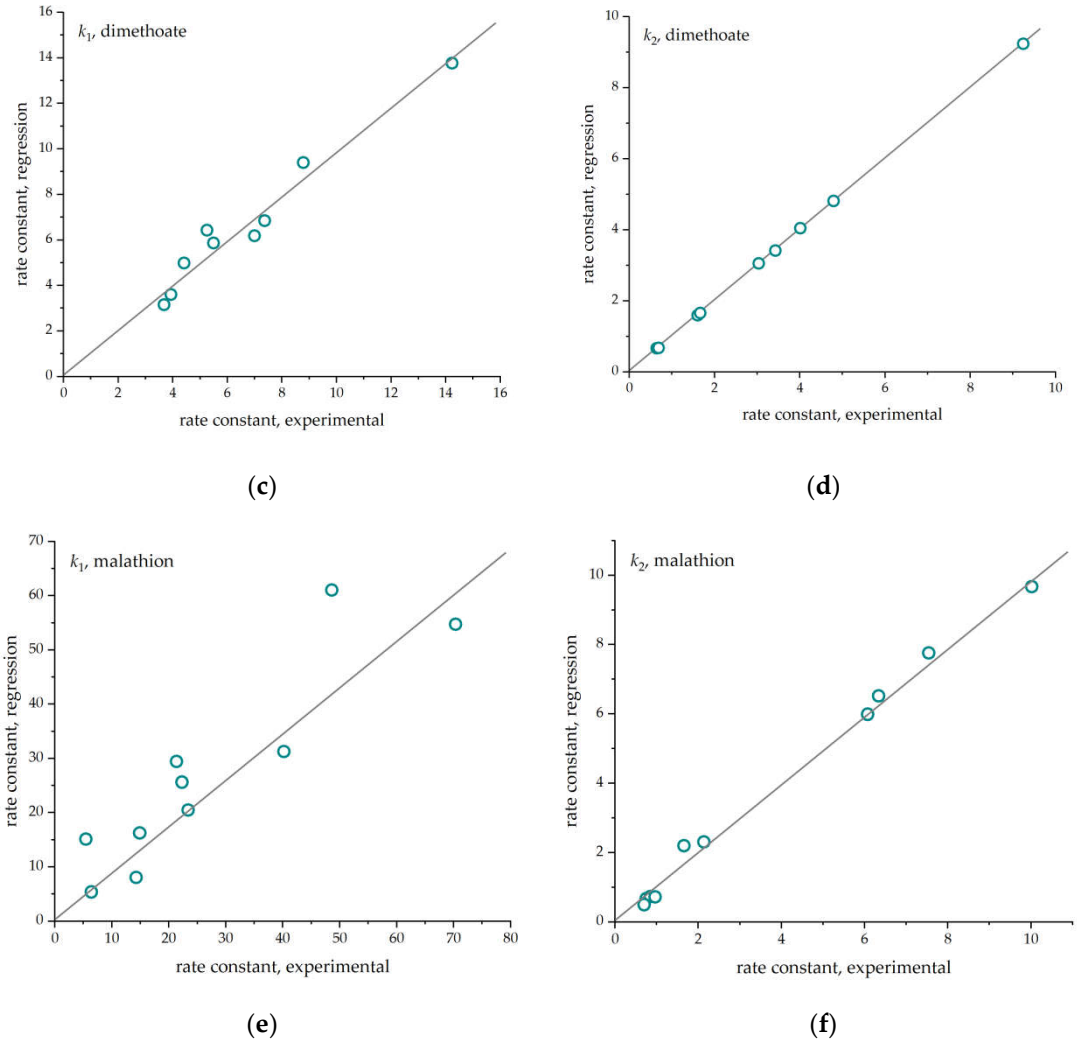

Figure 3. The results of multiple linear regression analysis (**a**) k_1 for chlorpyrifos, (**b**) k_2 for chlorpyrifos, (**c**) k_1 for dimethoate, (**d**) k_2 for dimethoate, (**e**) k_1 for malathion, (**f**) k_2 for malathion.

In order to analyze the impact of different materials' properties, we have to note that, besides the fact that chlorpyrifos has an aromatic ring, the molecules are of similar sizes, around 1 nm along the longest axis of a molecule but with some differences in branching (malathion) [21]. Thus, the accommodation of all three molecules into the pore structure of studied adsorbents should start from pores with a diameter above 1 nm. This could be even a bit larger as both adsorbent and adsorbate are solvated, which effectively reduces the pore diameter while increasing the dimensions of an adsorbate.

Now, if we consider the results of linear regression analysis (**Figure 3** and **Table A1**), we see that generally good predictions for adsorption rate constants are obtained, particularly pseudo-second-order kinetics in the cases of dimethoate and malathion. In both cases, three independent variables stand out. First, the model is very sensitive to the cumulative pore volumes for pores with diameters up to 2 nm and up to 4 nm, which positively correlate to the rate constants. Second, carbon content (**Table 1**) also seems to be a determinant for fast adsorption kinetics. As discussed before [20, 21], we believe that for studied materials, physisorption is operative. Thus positive correlation of carbon content with adsorption rate constants can be understood through the reduced amount of highly solvated domains, despite the fact that O atomic content also positively correlates to adsorption rate constants (much more for malathion compared to dimethoate). This can be due to dipole-dipole and electrostatic interactions, which can positively affect the adsorption rates. However, if some highly oxidized domains are present at the pore openings,

 doi:10.20944/preprints202211.0449.v1

they might block the entrance of pesticides into the pores, reducing the adsorption capacity and impeding the adsorption process rate.

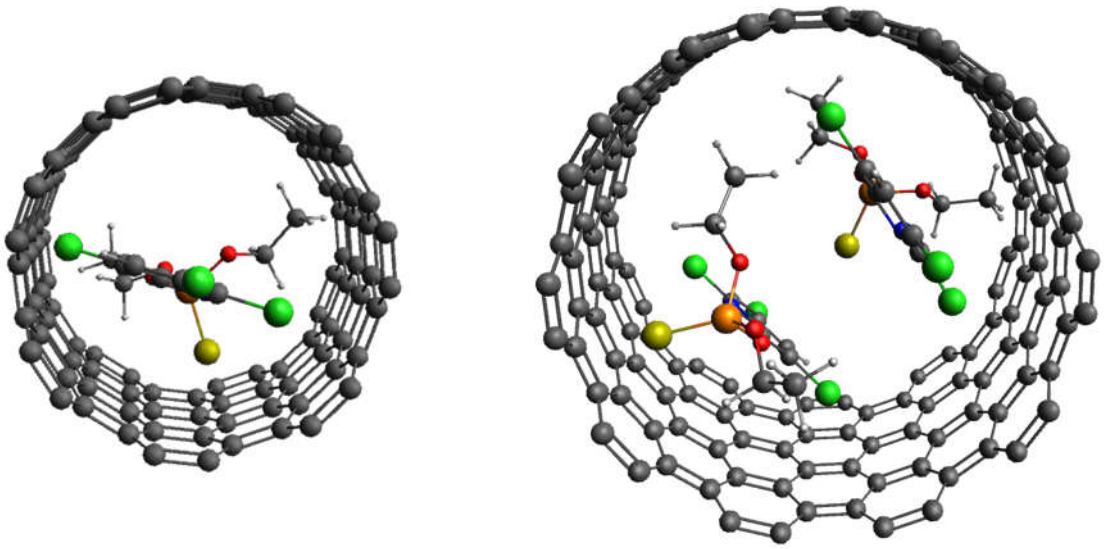

(**a**) (**b**)

Figure 4. Schematic representation of accommodation of chlorpyrifos molecules into pores of different diameters: (**a**) when pore diameter allows the entrance of only one molecule, (b) when the pore diameter is sufficient to place two chlorpyrifos molecules in the pore. Any pores with diameters between hypothetical cases of (a) and (b) can only accommodate one molecule along the pore diameter.

It is interesting to observe the role of cumulative pore volumes. Namely, we believe that the first limit corresponds to the entrance of individual molecules (including their solvation shells) into the pores in such a way that one molecule interacts with two opposite sides of the pore interior along the pore size diameter (**Figure 4, a**). The second situation (4 nm) corresponds to the case where the adsorbate molecule interacts with one side of the pore interior, but the pore diameter is large enough to accommodate two adsorbate molecules along the pore size diameter (**Figure 4, b**).

We believe that the diffusion of organophosphate molecules into the pore system of adsorbents must be spontaneous and without significant deformation of pesticide molecules, which would produce a large energy penalty in this process. To check for this assumption, we have performed semi-empirical quantum chemical calculations on chlorpyrifos inserted into the interior of (7,7) single-walled carbon nanotube (SWCNT), imitating the interior of a pore of studied ACFs. Such SWCNT has a diameter of 9.5 Å(if the length is infinite). For a finite-sized SWCNT we studied, the aliphatic part of the chlorpyrifos molecule gets "expelled" from the tube (**Figure 5a**), while both chlorpyrifos and nanotube undergo significant deformation (**Figure 5b**). The deformation energy of the chlorpyrifos molecule is 33 kJ mol^{-1}, while for SWCNT, it amounts to 710 kJ mol^{-1} (please note that this energy relates to one mole of finite-size SWCNTs used in this study). Even in the absence of a solvent shell, the entrance of chlorpyrifos into the pores smaller than 1 nm is rather unlikely to happen. Finally, we note that the obtained rate constants generally do not correlate with the adsorption capacities. Hence, to design proper adsorbents for different pesticides, one should consider properties that determine their adsorption capacities and fast adsorption kinetics under desired conditions.

Preprints (www.preprints.org) | NOT PEER-REVIEWED | Posted: 24 November 2022 doi:10.20944/preprints202211.0449.v1

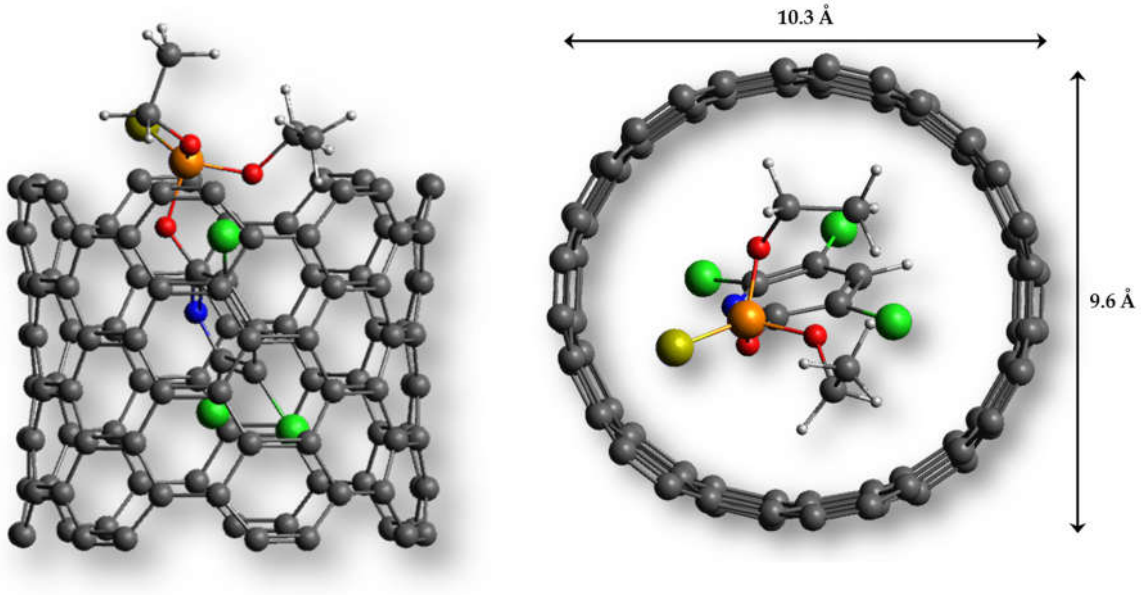

(**a**) (**b**)

Figure 5. Entrance of chlorpyrifos molecule into the SWCNT: (a) side view, (b) a view along the SWCNT (pore) axis; the deformation is visible as the SWCNT deviates from the circular shape.

4. Materials and Methods

4.1. Materials synthesis

Materials synthesis is described in [20] and reproduced here for the sake of completeness. Viscose fibers (1.7 dtex, 38 mm) were first dried for 24 h at 90°C and then impregnated in DAHP solutions of different concentrations for 15 min. The concentrations ranged from 0.0–75.7 mmol dm^{-3}, matching 0.00–10.00% DAHP in distilled water. After that, the fibers were dried for 24 h. Subsequently, carbonization was done in a chamber furnace (HTK8, Gero, Germany) under a nitrogen atmosphere. The samples were held isothermal for 20 min at 850 °C. The heating rate was 1.0 °C min^{-1}. Finally, the carbonized fibers were activated in a rotary kiln at 870 °C for 165 min in a CO_2 flow of 80 dm^3 h^{-1}. Previous studies have shown that additional washing is not needed due to the use of highly pure precursor fibers and an impregnation agent that does not introduce soluble components or change the pH value of the result ACF, in contrast to other chemical activation methods using [31, 32]. The samples are noted as DAHP-X, where X represents the concentration of DAHP used in the impregnation step.

4.2. Materials characterization

The morphology and the elemental composition of the ACF samples were investigated using a scanning electron microscope (PhenomProX, Thermo Fisher Scientific, USA) equipped with energy-dispersive X-ray spectroscopy (EDX).

The textural properties and specific surface area of materials were studied by N_2 isothermal adsorption (−196.15°C). For this purpose, a gas sorption system was used (AutosorbiQ, Quantachrome Instruments, USA). The specific surface area and derived pore size distribution (PSD) were calculated using the method of Brunauer-Emmett-Teller (BET) and the non-local density functional theory (NLDFT), respectively [33, 34].

4.3. Pesticide adsorption measurements

Batch adsorption experiments were done as stated below. First, materials were dispersed in double distilled water. The necessary volume of a pesticide stock solution (Pestanal, Sigma Aldrich, Denmark) was added to provide the final concentration of adsorbent and pesticide. Next, the container with the adsorbent and pesticide mixture was

 doi:10.20944/preprints202211.0449.v1

placed on a shaker (Orbital Shaker-Incubator ES-20, Grant-Bio, UK). It was held at 25 °C for chosen times. Then, the mixture was centrifuged and the supernatant was filtered. The concentration of organophosphates after adsorption (C_{eq}) was determined using Ultra Performance Liquid Chromatography (UPLC). Control experiments were performed in identical ways but without materials. It showed us that there was no pesticide degradation during the batch experiments. The pH of adsorbent and pesticide dispersions was monitored during the experiments. The measurement showed no differences between the samples. It is obvious that the differences in the kinetics of pesticide removal are due to their adsorption on studied materials and not because of chemical decomposition.

ACQUITY UPLC system (Waters, USA) with a tunable UV detector was used for UPLC measurements. It was controlled by the Empower software. ACQUITY UPLC™ BEH C18 column (1.7 μm, 100 mm × 2.1 mm, Waters, USA) was used. The analysis was done under isocratic conditions. The mobile phase consisted of acetonitrile and water (see ref. [21] for details).

4.4. Semi-empirical quantum chemical calculations

Semi-empirical calculations were done using the MOPAC2016 code [35] with the PM7 method [36]. A model of (7,7) SWCNT was constructed with 112 atoms to obtain the deformation energies of chlorpyrifos. Then chlorpyrifos molecule was placed into the tube, and full structural relaxation was done. After the relaxation, the system was split into nanotube and chlorpyrifos parts, and their molecular energies were calculated in on self-consistent cycle. Deformation energies were obtained by comparing the energy of fully relaxed chlorpyrifos/nanotube with the energy of chlorpyrifos/nanotube with the geometric corresponding to chlorpyrifos inserted into the nanotube.

5. Conclusions

In this contribution, we have analyzed the kinetics of chlorpyrifos, dimethoate, and malathion adsorption on a series of activated carbon fibers with diverse pore structures and chemical compositions. Adsorption data were processed to obtain pseudo-first and pseudo-second order rate constants. No particular trend was possible to extract in connection with only the studied materials' properties (integral pore volumes, the content of C, O, P). However, multiple linear regression can find the connection between the material's properties and adsorption kinetics. For dimethoate and malathion, pseudo-second-order kinetics, the regression analysis was particularly capable of giving reliable predictions for the rate constants. Among considered materials properties, cumulative pore volumes up to 2 nm and 4 nm and carbon content strongly positively correlated with rate constants. This is likely due to the interplay of the pesticide molecule sizes and pore diameters, allowing accommodating one or two pesticide molecules along the pore diameter. Theoretical calculations suggest that even in the absence of solvent, it is unlikely that pesticide molecules can enter pores with a diameter below 1 nm without significant deformation of the molecule (and the pore), requiring a large energy input for such process and making thermodynamically unfavorable. As the adsorption kinetics is not correlated to adsorption capacities, to design/choose adsorbents for a given application, one has to balance the properties that determine adsorption capacities and kinetics. For the studied pesticides, an ideal adsorbent is mesoporous carbon with a pore diameter around 4 nm (ideally unimodal pore size distribution) with a relatively low concentration of oxygen (and likely other heteroatoms) and largely preserved sp^2 domains.

Author Contributions: Conceptualization, I.A.P. and T.L.P.; methodology, I.A.P., S.B., C.U., C.F. and T.L.P.; software, I.A.P; formal analysis, A.J, V.M., T.T. and N.P.; investigation, A.J, V.M., T.T. and N.P.; resources, I.A.P., C.F. and T.L.P.; writing—original draft preparation, I.A.P., V.M., T.T. and T.L.P.; writing—review and editing, I.A.P., S.B., C.U., C.F. and T.L.P.; All authors have read and agreed to the published version of the manuscript.

Funding: The authors wish to thank the European Regional Development Fund (EFRE) and the province of Upper Austria for financial support of this study through the program IWB 2014–2020

(project BioCarb-K). T.L.P., A.J. V.M., T.T., and N.P. acknowledge the support provided by the Serbian Ministry of Education, Science and Technological Development (Contract number: 451-03-68/2022-14/200017). I.A.P. acknowledges the support provided by the Serbian Ministry of Education, Science and Technological Development (Contract number: 451-03-68/2022-14/200146).

Data Availability Statement: Data are available upon reasonable request.

Conflicts of Interest: The authors declare no conflict of interest.

Appendix A

Table A1. Multiple linear regression parameters. See Section 3 for the assignment of each parameter to a given independent variable.

model	A_1	A_2	A_3	A_4	A_5	A_6	A_7	A_8	R^2
CPF-1	16.4	0.5	27.4	−140.5	112.4	−0.6	−1.9	3.0	0.97
CPF-2	−1.9	−0.8	−2.0	4.2	−2.0	1.5	0.2	−0.3	0.73
DMT-1	26.6	48.7	−146.1	404.0	−307.1	−1.3	−1.7	18.5	0.93
DMT-2	−99.6	40.4	−137.3	422.0	−329.6	37.4	8.6	1.8	0.9999
MLT-1	431.9	−62.0	−485.7	2202.0	−1726.5	−47.4	−6.6	30.6	0.68
MLT-2	−82.6	57.7	−234.0	765.7	−563.9	25.1	0.3	−7.5	0.99

References

1. Miodovnik, A., Prenatal Exposure to Industrial Chemicals and Pesticides and Effects on Neurodevelopment☆, in *Encyclopedia of Environmental Health (Second Edition)*, Nriagu, J., Editor. **2019**, Elsevier: Oxford. p. 342-352.
2. Kwong, T.C., Organophosphate Pesticides: Biochemistry and Clinical Toxicology. *Therapeutic Drug Monitoring* **2002,** *24*, 144-149.
3. Lazarević-Pašti, T., Organophosphates: Detection, Exposure and Occurrence. Volume 1: Impact on Health and the Natural Environment. **2022**, Nova Science Publishers, New York.
4. Lazarević-Pašti, T.; Anićijević, V.; Baljozović, M.; Anićijević, D.V.; Gutić, S.; Vasić, V.; Skorodumova, N.V.; Pašti, I.A. The impact of the structure of graphene-based materials on the removal of organophosphorus pesticides from water. *Environmental Science: Nano* **2018,** *5*, 1482-1494. 10.1039/C8EN00171E
5. Lazarević-Pašti, T.D.; Pašti, I.A.; Jokić, B.; Babić, B.M.; Vasić, V.M. Heteroatom-doped mesoporous carbons as efficient adsorbents for removal of dimethoate and omethoate from water. *RSC Advances* **2016,** *6*, 62128-62139. 10.1039/C6RA06736K
6. Anicijevic, V.; Lazarević-Pašti, T.; Vasic Anicijevic, D.; Karkalic, R. Esters of Organophosphorus Acids - Toxicity, Application and Removal from the Environment. *Scientific Technical Review* **2019**. 10.5937/str1903015A
7. Soffian, M.S.; Abdul Halim, F.Z.; Aziz, F.; A. Rahman, M.; Mohamed Amin, M.A.; Awang Chee, D.N. Carbon-based material derived from biomass waste for wastewater treatment. *Environmental Advances* **2022,** *9*, 100259. https://doi.org/10.1016/j.envadv.2022.100259
8. Haghseresht, F.; Nouri, S.; Finnerty, J.J.; Lu, G.Q. Effects of Surface Chemistry on Aromatic Compound Adsorption from Dilute Aqueous Solutions by Activated Carbon. *The Journal of Physical Chemistry B* **2002,** *106*, 10935-10943.10.1021/jp025522a
9. Sabzehmeidani, M.M.; Mahnaee, S.; Ghaedi, M.; Heidari, H.; Roy, V.A.L. Carbon based materials: a review of adsorbents for inorganic and organic compounds. *Materials Adv* **2021,** *2*, 598-627. 10.1039/D0MA00087F
10. Moreno-Castilla, C. Adsorption of Organic Molecules from Aqueous Solutions on Carbon Materials. *Carbon* **2004,** *42*, 83-94. 10.1016/j.carbon.2003.09.022
11. Al-Degs, Y.S.; El-Barghouthi, M.I.; El-Sheikh, A.H.; Walker, G.M. Effect of solution pH, ionic strength, and temperature on adsorption behavior of reactive dyes on activated carbon. *Dyes and Pigments* **2008,** *77*, 16-23. https://doi.org/10.1016/j.dyepig.2007.03.001
12. Newcombe, G.; Drikas, M.; Hayes, R. Influence of characterised natural organic material on activated carbon adsorption: II. Effect on pore volume distribution and adsorption of 2-methylisoborneol. *Wat Res* **1997,** *31*, 1065-1073. https://doi.org/10.1016/S0043-1354(96)00325-9
13. Dubinin, M.M. The Potential Theory of Adsorption of Gases and Vapors for Adsorbents with Energetically Nonuniform Surfaces. *Chemical Rev* **1960,** *60*, 235-241. 10.1021/cr60204a006
14. Sing, K.S.W. Physisorption of nitrogen by porous materials. *Journal of Porous Mat* **1995,** *2*, 5-8. 10.1007/BF00486564
15. Li, L.; Quinlivan, P.A.; Knappe, D.R.U. Effects of activated carbon surface chemistry and pore structure on the adsorption of organic contaminants from aqueous solution. *Carbon* **2002,** *40*, 2085-2100. https://doi.org/10.1016/S0008-6223(02)00069-6
16. Wang, S.; Zhu, Z.H.; Coomes, A.; Haghseresht, F.; Lu, G.Q. The physical and surface chemical characteristics of activated carbons and the adsorption of methylene blue from wastewater. *Journal of colloid and interface science* **2005,** *284*, 440-446. 10.1016/j.jcis.2004.10.050
17. Bandosz, T.J. Activated carbon surfaces in environmental remediation. **2006**: Elsevier.

18. Yang, K.; Xing, B. Adsorption of organic compounds by carbon nanomaterials in aqueous phase: Polanyi theory and its application. *Chem Rev* **2010,** *110*, 5989-6008. 10.1021/cr100059s
19. Yang, K.; Wu, W.; Jing, Q.; Zhu, L. Aqueous adsorption of aniline, phenol, and their substitutes by multi-walled carbon nanotubes. *Environmental science & technology* **2008,** *42*, 7931-7936. 10.1021/es801463v
20. Jocić, A.; Breitenbach, S.; Bajuk-Bogdanović, D.; Pašti, I.A.; Unterweger, C.; Fürst, C.; Lazarević-Pašti, T. Viscose-Derived Activated Carbons Fibers as Highly Efficient Adsorbents for Dimethoate Removal from Water. *Molecules* **2022,** *27*, 1477. 10.3390/molecules27051477
21. Jocić, A.; Breitenbach, S.; Pašti, I.A.; Unterweger, C.; Fürst, C.; Lazarević-Pašti, T. Viscose-derived activated carbons as adsorbents for malathion, dimethoate, and chlorpyrifos-screening, trends, and analysis. *Environmental science and pollution research international* **2022,** *29*, 35138-35149. 10.1007/s11356-022-18721-1
22. Kostoglou, M.; Karapantsios, T.D. Why Is the Linearized Form of Pseudo-Second Order Adsorption Kinetic Model So Successful in Fitting Batch Adsorption Experimental Data? *Colloids and Interfaces* **2022,** *6*, 55. https://doi.org/10.3390/colloids6040055
23. Blachnio, M.; Derylo-Marczewska, A.; Seczkowska, M. Influence of Pesticide Properties on Adsorption Capacity and Rate on Activated Carbon from Aqueous Solution. **2019**. IntechOpen. 10.5772/intechopen.88726
24. Derylo-Marczewska, A.; Blachnio, M.; Marczewski, A.W.; Seczkowska, M.; Tarasiuk, B. Phenoxyacid pesticide adsorption on activated carbon – Equilibrium and kinetics. *Chemosphere* **2019,** *214*, 349-360. https://doi.org/10.1016/j.chemosphere.2018.09.088
25. Marczewski, A.W.; Seczkowska, M.; Deryło-Marczewska, A.; Blachnio, M. Adsorption equilibrium and kinetics of selected phenoxyacid pesticides on activated carbon: effect of temperature. *Adsorption* **2016,** *22*, 777-790. 10.1007/s10450-016-9774-0
26. Yahia, M.; Elzaref, A.; Awad, M.; Tony, A.; Elfeky, A. Efficient adsorption of chlorpyrifos onto modified activated carbon by gamma irradiation; a plausible adsorption mechanism. *Zeitschrift für Physikalische Chemie* **2021,** *236*. 10.1515/zpch-2020-1765
27. Vigneshwaran, S.; Preethi, J.; Meenakshi, S. Removal of chlorpyrifos, an insecticide using metal free heterogeneous graphitic carbon nitride (g-C3N4) incorporated chitosan as catalyst: Photocatalytic and adsorption studies. *International Journal of Biological Macromolecules* **2019,** *132*, 289-299. https://doi.org/10.1016/j.ijbiomac.2019.03.071
28. Bondžić, A.M.; Lazarević Pašti, T.D.; Pašti, I.A.; Bondžić, B.P.; Momčilović, M.D.; Loosen, A.; Parac-Vogt, T.N. Synergistic Effect of Sorption and Hydrolysis by NU-1000 Nanostructures for Removal and Detoxification of Chlorpyrifos. *ACS Applied Nano Materials* **2022,** *5*, 3312-3324. 10.1021/acsanm.1c03863
29. Ndifreke, W.E.; Pasaoglulari Aydinlik, N. KOH modified Thevetia peruviana shell activated carbon for sorption of dimethoate from aqueous solution. *Journal of Environmental Science and Health, Part B* **2019,** *54*, 1-13. 10.1080/03601234.2018.1501143
30. Habila, M.A.; Alothman, Z.A.; Al-Tamrah, S.A.; Ghafar, A.A.; Soylak, M. Activated carbon from waste as an efficient adsorbent for malathion for detection and removal purposes. *Journal of Industrial and Engineering Chemistry* **2015,** *32*, 336-344. https://doi.org/10.1016/j.jiec.2015.09.009
31. Wang, J.; Kaskel, S. KOH activation of carbon-based materials for energy storage. *Journal of Materials Chemistry* **2012,** *22*, 23710-23725. 10.1039/C2JM34066F
32. Caturla, F.; Molina-Sabio, M.; Rodriguez-Reinoso, F. Preparation of activated carbon by chemical activation with ZnCl2. *Carbon* **1991,** *29*, 999-1007. https://doi.org/10.1016/0008-6223(91)90179-M
33. Bardestani, R.; Patience, G.S.; Kaliaguine, S. Experimental methods in chemical engineering: specific surface area and pore size distribution measurements—BET, BJH, and DFT. *The Canadian Journal of Chemical Engineering* **2019,** *97*, 2781-2791. https://doi.org/10.1002/cjce.23632
34. Kupgan, G.; Liyana-Arachchi, T.P.; Colina, C.M., NLDFT Pore Size Distribution in Amorphous Microporous Materials. *Langmuir* **2017,** *33*, 11138-11145. 10.1021/acs.langmuir.7b01961
35. Stewart, J.J., Mopac2016. Stewart Computational Chemistry: Colorado Springs, CO, USA **2016,** 650
36. Stewart, J.J., Optimization of parameters for semiempirical methods VI: more modifications to the NDDO approximations and re-optimization of parameters. *Journal of molecular modeling* **2013,** *19*, 1-32. 10.1007/s00894-012-1667-x